ACS APPLIED MATERIALS & INTERFACES

Research Article

www.acsami.org

Transformation of Ag Nanocubes into Ag–Au Hollow Nanostructures with Enriched Ag Contents to Improve SERS Activity and Chemical Stability

Yin Yang,[†,‡] Qiang Zhang,[†] Zheng-Wen Fu,[‡] and Dong Qin*[,†]

[†]School of Materials Science and Engineering, Georgia Institute of Technology, Atlanta, Georgia 30332, United States

[‡]Department of Materials Science, Fudan University, Shanghai 200433, P. R. China

Supporting Information

ABSTRACT: We report a strategy to complement the galvanic replacement reaction between Ag nanocubes and $HAuCl_4$ with co-reduction by ascorbic acid (AA) for the formation of Ag–Au hollow nanostructures with greatly enhanced SERS activity. Specifically, in the early stage of synthesis, the Ag nanocubes are sharpened at corners and edges because of the selective deposition of Au and Ag atoms at these sites. In the following steps, the pure Ag in the nanocubes is constantly converted into Ag^+ ions to generate voids owing to the galvanic reaction with $HAuCl_4$, but these released Ag^+ ions are immediately reduced back to Ag atoms and are co-deposited with Au atoms onto the nanocube templates. We observe distinctive SERS properties for the Ag–Au hollow nanostructures at visible and near-infrared excitation wavelengths. When plasmon damping is eliminated by using an excitation wavelength of 785 nm, the SERS activity of the Ag–Au hollow nanostructures is 15- and 33-fold stronger than those of the original Ag nanocubes and the Ag–Au nanocages prepared by galvanic replacement without co-reduction, respectively. Additionally, Ag–Au hollow nanostructures embrace considerably improved stability in an oxidizing environment such as aqueous H_2O_2 solution. Collectively, our work suggests that the Ag–Au hollow nanostructures will find applications in SERS detection and imaging.

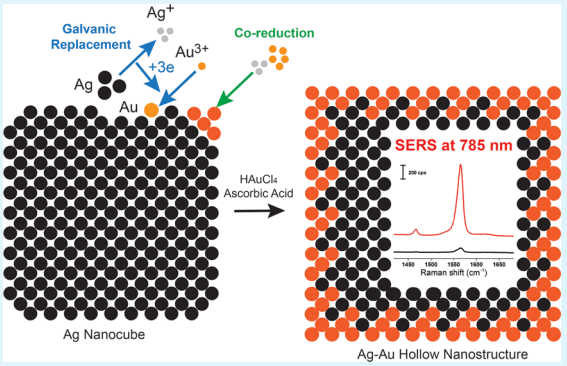

KEYWORDS: *bimetallic nanostructures, co-reduction, galvanic replacement, surface-enhanced Raman scattering (SERS)*

1. INTRODUCTION

Surface-enhanced Raman scattering (SERS), an exquisite vibrational spectroscopic technique, relies on the localized surface plasmon resonance (LSPR) and enhancement of electromagnetic fields around metal nanostructures to increase drastically the Raman scattering cross sections of molecules in close proximity to the nanostructures.[1−6] It has been documented that Ag nanostructures have excellent LSPR properties for SERS applications.[7−9] For example, Ag nanocubes embrace SERS properties with enhancement factors up to 10^6 at visible-excitation wavelengths for highly sensitive detection of chemical or biological species.[10−12] Unfortunately, elemental Ag is highly susceptible to oxidation under conditions that involve oxidants, halide ions, acids, water, UV irradiation, and heating.[13−17] Such chemical instability often results in changes to the morphology of Ag nanostructures, particularly at corners and edges with high surface free energies, and ultimately compromises their performance in SERS.[18]

One potential solution to improve the chemical stability of Ag nanostructures is to form an alloy with a more stable metal such as Au.[19,20] However, it is difficult to form Ag–Au alloys by reducing their precursors simultaneously in a solution phase because of their substantial differences in reactivity.[21,22] As an alternative, the galvanic replacement reaction between elemental Ag and a Au precursor such as $HAuCl_4$ has been extensively used to produce hollow nanostructures made of Ag–Au alloys together with pores in the walls.[23−26] Although the Ag–Au hollow nanostructures exhibit LSPR peaks tunable from 500 to 1200 nm,[23,25,27] their SERS performance was extremely poor with no measurable activity with excitation at 514 nm.[28] Part of the problem arises from the destructive nature of the galvanic replacement reaction that involves the deposition of one Au atom at the expense of three Ag atoms from the template. Such a significant loss of Ag during the formation of Ag–Au hollow nanostructures could account for their diminished SERS activity.

One strategy to alleviate the negative impact of galvanic replacement reaction on the SERS performance of the Ag–Au hollow structures is to introduce a strong reducing agent, such as ascorbic acid (AA),[29] to reduce the Ag^+ ions originating from the galvanic replacement back to Ag atoms and then co-deposit them with Au atoms onto the Ag templates. Previously, several

Received: January 24, 2014
Accepted: January 29, 2014
Published: January 29, 2014

   dx.doi.org/10.1021/am500506j | ACS Appl. Mater. Interfaces 2014, 6, 3750−3757

groups have explored a similar concept for backfilling the pores in the Ag triangular plates that resulted from a galvanic replacement reaction with $HAuCl_4$.[30−32] Others have also introduced a reducing agent to couple with the galvanic replacement reaction for the generation of ultrathin Au nanoframes on the surfaces of Ag decahedrons and octahedrons[33,34] or Au−Pd, Cu−M (M = Au, Pt, or Pd) bimetallic nanostructures.[35,36] In this work, we demonstrate that the galvanic replacement reaction between Ag nanocubes and $HAuCl_4$ could be combined with co-reduction by AA for the formation of Ag−Au hollow nanostructures without losing the Ag content. We confirm that the reduction of Ag^+ ions originating from the galvanic replacement could effectively retain >80% of the elemental Ag to the walls of the Ag−Au hollow nanostructures. More significantly, with an excitation wavelength of 785 nm to eliminate plasmon dephasing associated with interband transition of Au at 2.5 eV (~500 nm),[37] the Ag−Au hollow nanostructures exhibit SERS activity 15- and 33-fold stronger than those of the original Ag nanocubes and the Ag−Au nanocages prepared using galvanic replacement without co-reduction, respectively. These Ag−Au hollow nanostructures also embrace improved stability in an oxidizing environment. All of these unique attributes make the Ag−Au hollow nanostructures attractive for SERS detection and imaging.

2. RESULTS AND DISCUSSION

2.1. Formation of Ag−Au Hollow Nanostructures with Enrichment in Ag Content. In a typical synthesis, we dispersed Ag nanocubes in an aqueous solution containing poly(vinyl pyrrolidone) (PVP, a capping agent and colloidal stabilizer) and ascorbic acid (AA, a reductant) followed by the titration of an aqueous $HAuCl_4$ solution using a syringe pump at room temperature. Differing from the previous procedure for galvanic replacement, the inclusion of AA allows the generation of Au and Ag atoms through the co-reduction of $AuCl_4^-$ ions and the Ag^+ ions originating from the galvanic replacement between Ag and $AuCl_4^-$ followed by their co-deposition on the Ag nanocubes. To monitor the changes in morphology and composition in the course of reaction, we took aliquots of samples from the solution at different time points to characterize products using transmission electron microscopy (TEM), high-angle annular dark-field scanning transmission electron microscopy (HAADF-STEM), energy-dispersive X-ray (EDX) spectroscopy, inductively coupled plasma mass spectrometry (ICP-MS), and UV−vis−NIR spectroscopy.

Figure 1 shows TEM images and schematic illustrations (insets) of Ag nanocubes after they reacted with different volumes of $HAuCl_4$ in the presence of AA. With the addition of 0.05 mL of $HAuCl_4$, the nanocubes were sharpened at the corners and edges as a result of metal deposition at these sites (Figure 1A). The edge length of the nanocubes was measured as 39.2 ± 2.6 nm, essentially identical to the size of the original Ag nanocubes (Figures S1). Upon removal of the pure Ag remaining in the nanocubes using an aqueous H_2O_2 solution, we observed the formation of Ag−Au cubic nanoframes with a thickness of 3.6 ± 0.2 nm for the ridges (Figure 1E) and a mole fraction of 70% for Ag. In comparison, galvanic replacement alone with 0.05 mL of $HAuCl_4$ led to the formation of visible voids in the nanocubes (Figure S2A). These results suggest that, in the early stage, co-reduction of the added $AuCl_4^-$ ions and the Ag^+ ions originating from the Ag nanocubes resulting from galvanic replacement led to the selective deposition of Au

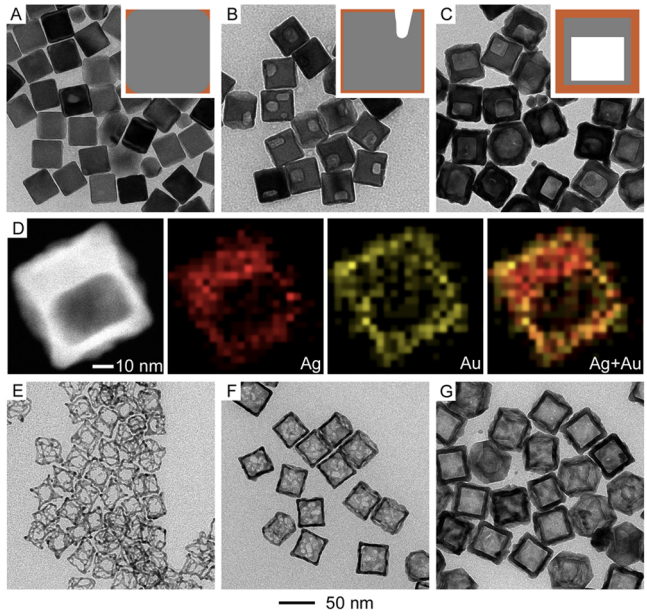

Figure 1. TEM images and illustrations (insets) of Ag nanocubes after reacting with different volumes of 0.2 mM $HAuCl_4$ solution in the presence of AA: (A) 0.05, (B) 0.2, and (C) 0.6 mL. (D) HAADF-STEM and EDX mapping analysis of a nanocube after reacting with 0.6 mL $HAuCl_4$. (E−G) TEM images of nanostructures that were obtained by etching the structures shown in panels A−C with an excess amount of H_2O_2 solution.

and Ag atoms at the corners and edges of Ag nanocubes because their side faces were passivated by PVP.[38,39] As the reaction proceeded with an increase of $HAuCl_4$ to 0.2 mL in the presence of AA, the Ag nanocubes were transformed into nanocubes with voids in the interiors (Figure 1B). These voids were smaller than those prepared using galvanic replacement alone in the absence of AA (Figure S2B). The edge length of the nanocubes was increased from 39.2 ± 2.6 to 44.0 ± 1.7 nm. Upon removal of the pure Ag remaining in the nanocubes with an aqueous H_2O_2 solution, we noticed the formation of Ag−Au nanocages with multiple pores in the walls (Figure 1F). These results support our argument that the co-reduction of $AuCl_4^-$ and Ag^+ by AA and the co-deposition of resultant Au and Ag atoms onto the surface of Ag nanocubes occurred simultaneously, accompanied by galvanic replacement between Ag and $AuCl_4^-$ to continuously release Ag^+ ions into the solution and enlarge the voids in the interiors.

With additional increase of $HAuCl_4$ to 0.6 mL in the presence of AA, the Ag nanocubes were transformed into Ag−Au hollow nanostructures with a further increase in edge length to 50.5 ± 2.2 nm (Figure 1C). It is worth emphasizing that these Ag−Au hollow nanostructures are different from Ag−Au nanocages prepared using a galvanic replacement alone (Figure S2C). Specifically, with the involvement of co-reduction by AA, the mole fraction of Ag was increased from 65 to 76%, and the porosity of the walls was decreased. At this stage, galvanic replacement had consumed most of the Ag in the nanocubes together with the enlargement of voids. Elemental mapping of a Ag−Au hollow nanostructure shows the formation of Ag−Au alloy walls (Figure 1D) together with some pure Ag remaining inside the nanocube. By removing the residual Ag in the nanocubes with H_2O_2, we confirmed the formation of Ag−Au hollow nanostructures with no pores on their surfaces (Figure 1G). We also found that the thickness of the Ag−Au walls was

dx.doi.org/10.1021/am500506j | ACS Appl. Mater. Interfaces 2014, 6, 3750−3757

increased from 3.1 ± 0.2 to 7.2 ± 0.4 nm because of the retention of Ag content to the walls. These results suggest that co-reduction could inhibit the dealloying process associated with the galvanic replacement, leading to the formation of Ag–Au hollow nanostructures with nonporous walls made of a Ag–Au alloy.

When the reaction was continued with the addition of 1.0 and 1.5 mL $HAuCl_4$, we observed the formation of Ag–Au hollow nanostructures with an increase in wall thickness (Figure 2). In comparison, galvanic replacement alone with 1.0

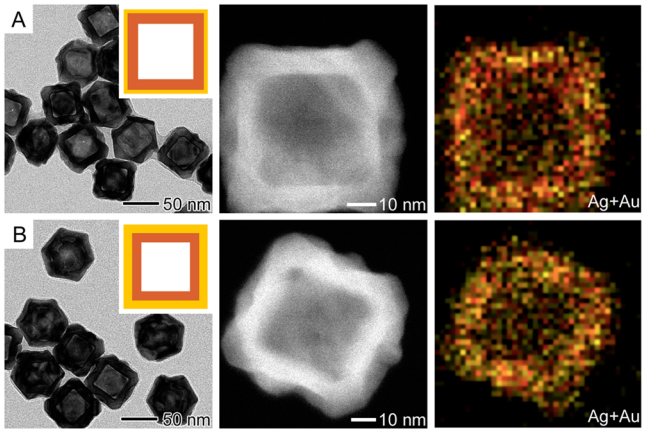

Figure 2. TEM images, illustrations (insets), HAADF-STEM images, and EDX mapping analyses of Ag nanocubes after reaction with two different volumes of 0.2 mM aqueous $HAuCl_4$ solution in the absence of AA: (A) 1.0 and (B) 1.5 mL.

mL of $HAuCl_4$ led to the formation of nanocages with hollow interiors, truncated corners, and porous walls (Figure S2D). Again, we validate that the co-reduction of $AuCl_4^-$ and Ag^+ by AA could effectively eliminate the intrinsic dealloying process associated with galvanic replacement reaction. Once all of the pure Ag in the nanocubes had been consumed, galvanic replacement would be terminated followed by the reduction of the remaining $AuCl_4^-$ ions in the reaction solution by AA to promote epitaxial deposition of Au on the {100} facets for the formation of Au-coated Ag–Au hollow nanostructures.

2.2. Retention of Ag Because of Co-Reduction by AA. To understand the mechanistic details involved in the formation of Ag–Au hollow nanostructures, we used ICP-MS to measure the contents of Ag and Au in the as-prepared samples when Ag nanocubes were reacted with different volumes of $HAuCl_4$ in the presence and absence of AA, respectively. Specifically, the solid samples were collected by centrifugation and removal of supernatant followed by dissolution in aqua regia for ICP-MS analysis. Figure 3 shows the amounts of Ag and Au in the solid samples after the Ag nanocubes had reacted with different volumes of $HAuCl_4$. In the presence and absence of AA, the two lines show similar trends (the amount of Au increased linearly with the volume of $HAuCl_4$). In both cases, the added $AuCl_4^-$ was reduced and deposited onto the Ag nanocubes, even though it is still not clear if the deposition involves Au atoms directly or the reduction of $AuCl_4^-$ pre-adsorbed on the surface. Unlike the Au content, the amount of Ag exhibits two distinctive trends. When Ag nanocubes reacted with $HAuCl_4$ without co-reduction, the amount of Ag decreased linearly from 41.1 to 5.7 μg as the volume of $HAuCl_4$ was increased to 1.0 mL, indicating that galvanic replacement accounts for an 87% loss of

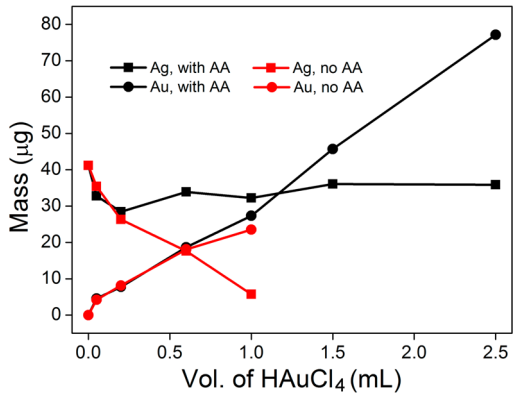

Figure 3. Au and Ag contents in the as-prepared Ag–Au nanostructures when Ag nanocubes were reacted with different volumes of 0.2 mM aqueous $HAuCl_4$ solution in the presence and absence of AA.

Ag from the original Ag nanocubes. Alternatively, when the galvanic replacement reaction was coupled with co-reduction, the amount of Ag decreased linearly from 41.1 to 32.8 and 28.5 μg with the addition of 0.05 and 0.2 mL of $HAuCl_4$ solution, respectively. However, when the volume of $HAuCl_4$ was further increased from 0.2 to 2.5 mL, the amount of Ag remained at a relatively stable level of 34.0 μg, which corresponds to a 17% loss of Ag from the original Ag nanocubes. Consistent with the TEM images shown in Figures 1 and 2, ICP-MS results verify that >80% of the Ag^+ ions released from the galvanic replacement could be effectively reduced back to Ag atoms by AA and ultimately re-deposited onto the Ag nanocubes.

2.3. Characterization of LSPR Properties. Both Ag and Au nanostructures exhibit distinctive LSPR properties with a strong dependence on parameters that include internal structure (solid versus hollow), morphology, and composition.[8] In this work, we used UV–vis–NIR spectroscopy to characterize the LSPR properties associated with changes to these three parameters when the Ag nanocubes reacted with $HAuCl_4$ for their transformation into Ag–Au hollow nanostructures. Figure 4A shows the UV–vis–NIR spectra collected from aqueous dispersions of Ag nanocubes before and after they had reacted with different volumes of aqueous $HAuCl_4$ in the presence of AA. With the addition of 0.05 mL of $HAuCl_4$, the LSPR peak of the Ag nanocubes was slightly shifted from 436 to 461 nm, with the width of peak remaining unchanged. The subtle change in LSPR reflects the transformation of Ag nanocubes as they became sharper because of the selective deposition of metal atoms at their corners and edges (Figure 1A). With the addition of 0.2 mL of $HAuCl_4$, the LSPR peak position was further red-shifted to 491 nm together with a decrease in intensity and broadening in peak width. The peak broadening suggests the formation of voids in the interiors (Figure 1B).[23] When the volume of $HAuCl_4$ was increased to 0.6 mL, the Ag–Au hollow nanostructures (Figure 1C) exhibited a major peak at 573 nm together with a shoulder peak positioned at 502 nm. With a further increase in $HAuCl_4$, the deposition of Au allowed the formation of thick shells of Au on the Ag–Au hollow nanostructures (Figure 2). As a result, the major LSPR peak was further red-shifted from 573 to 596 nm at 1.0 mL of $HAuCl_4$ followed by a change in intensity at 1.5 mL of $HAuCl_4$. We also collected the UV–vis–NIR spectra of Ag nanocubes after they were reacted with different volumes of aqueous $HAuCl_4$ in the absence of AA (Figure 4B). Consistent with

dx.doi.org/10.1021/am500506j | ACS Appl. Mater. Interfaces 2014, 6, 3750–3757

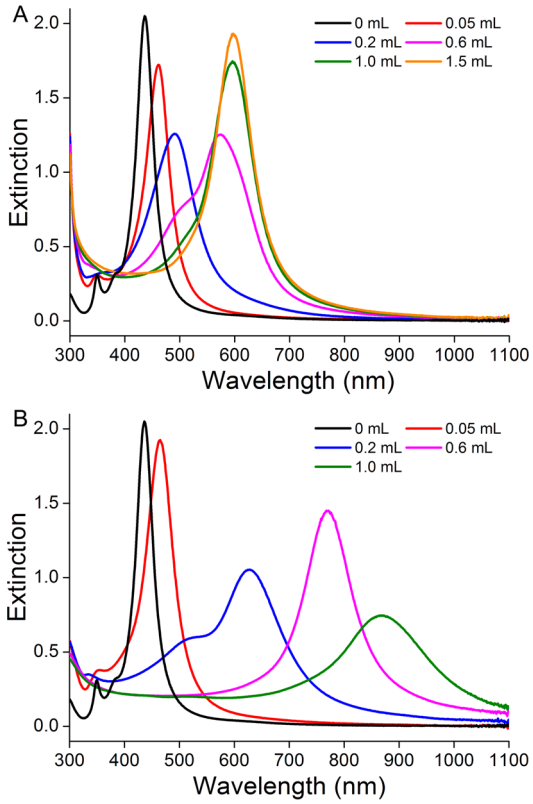

Figure 4. UV–vis–NIR spectra of aqueous suspensions of Ag nanocubes before and after reacting with different volumes of 0.2 mM aqueous $HAuCl_4$ solution in the presence (A) and absence (B) of AA.

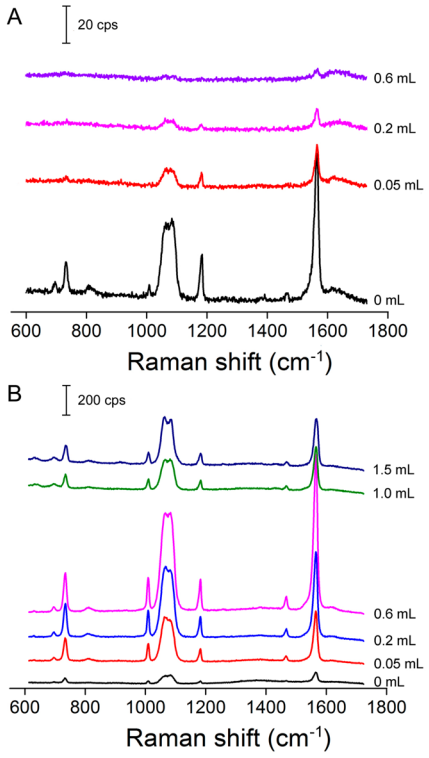

Figure 5. SERS spectra taken from 1,4-BDT adsorbed on Ag nanocubes before and after reacting with different volumes of 0.2 mM aqueous $HAuCl_4$ solution in the presence of AA. The spectra were recorded with excitation wavelengths at (A) 532 and (B) 785 nm. Note that the SERS signals were different by 10-fold between the spectra in panels A and B.

previous work, the LSPR peak was constantly red-shifted into the near-infrared region because of the formation of Ag–Au nanocages as the volume of $HAuCl_4$ increased.[23] Collectively, these results indicate that the co-reduction of $AuCl_4^-$ and Ag^+ by AA could effectively retard the dealloying process and ultimately help to retain Ag effectively to the walls of Ag–Au hollow nanostructures.

2.4. Enhancement in SERS Activity Because of Ag Enrichment. We evaluated the SERS properties of Ag nanocubes before and after they had reacted with different volumes of $HAuCl_4$ solution in the presence of AA. Figure 5 shows the SERS spectra of 1,4-benzenedithiol (1,4-BDT) molecules adsorbed on the surfaces of Ag nanocubes and Ag–Au hollow nanostructures at excitation wavelengths of 532 and 785 nm, respectively. Specifically, Figure 5A shows that the intensity of SERS peak at 1562 cm^{-1} (the benzene ring mode 8a) decreases rapidly to zero with excitation at 532 nm when the Ag nanocubes were reacted with different amounts of $HAuCl_4$ in the presence of AA. In contrast, with excitation at 785 nm, Figure 5B indicates a significant increase in the SERS peak at 1562 cm^{-1} as the reaction progressed with different amounts of $HAuCl_4$. Most interestingly, we found that a simple titration of different volumes of $HAuCl_4$ into the suspension of Ag nanocubes allowed us to optimize their SERS activity. For example, the SERS activity reached a maximum value when the Ag nanocubes were reacted with 0.6 mL of $HAuCl_4$ in the presence of AA to form Ag–Au hollow nanostructures with an improvement factor of 15 in SERS activity in comparison with the Ag nanocubes.

For the first time, we observed distinctive SERS properties at visible and near-infrared excitation wavelengths for the Ag–Au hollow nanostructures. Our findings suggest some important factors that determine the SERS activity of Ag and Au nanostructures. We noticed that the visible laser excitation at 532 nm promoted a relatively strong SERS activity for Ag nanocubes but not for the Ag–Au hollow nanostructures, which is consistent with previous findings.[28] Because the interband transition edges of Au and Ag are located at 2.5 (~500 nm) and 3.8 eV (~330 nm), respectively,[37] the inclusion of Au into Ag nanostructures may result in a stronger plasmon damping at visible-excitation wavelengths and thereby attenuate SERS intensity. When the excitation wavelength was switched to 785 nm to eliminate the plasmon damping, the SERS activity of the Ag–Au hollow nanostructures became 15-fold stronger than that of the Ag nanocubes. Additionally, we determined that the SERS activity could be optimized by maneuvering the morphology and composition. For example, we observed enhancement in SERS activity for the Ag nanocubes when their corners and edges were sharpened because of the selective deposition of metal atoms upon the addition of 0.05 mL of $HAuCl_4$ in the presence of AA (Figure 2B). The sharp corners on nanocubes could serve as hot spots with extremely large electric-field enhancement for the generation of incredibly high SERS enhancement.[8]

We also discovered that the enrichment of Ag in the Ag–Au hollow nanostructures could drastically increase the SERS activity. To validate our argument, we collected SERS spectra from Ag nanocubes that had been reacted with different volumes of $HAuCl_4$ in the absence of AA (Figure S3). With the addition of 0.6 mL of $HAuCl_4$, the Ag–Au hollow nanostructures produced in presence of AA showed SERS

dx.doi.org/10.1021/am500506j | ACS Appl. Mater. Interfaces 2014, 6, 3750–3757

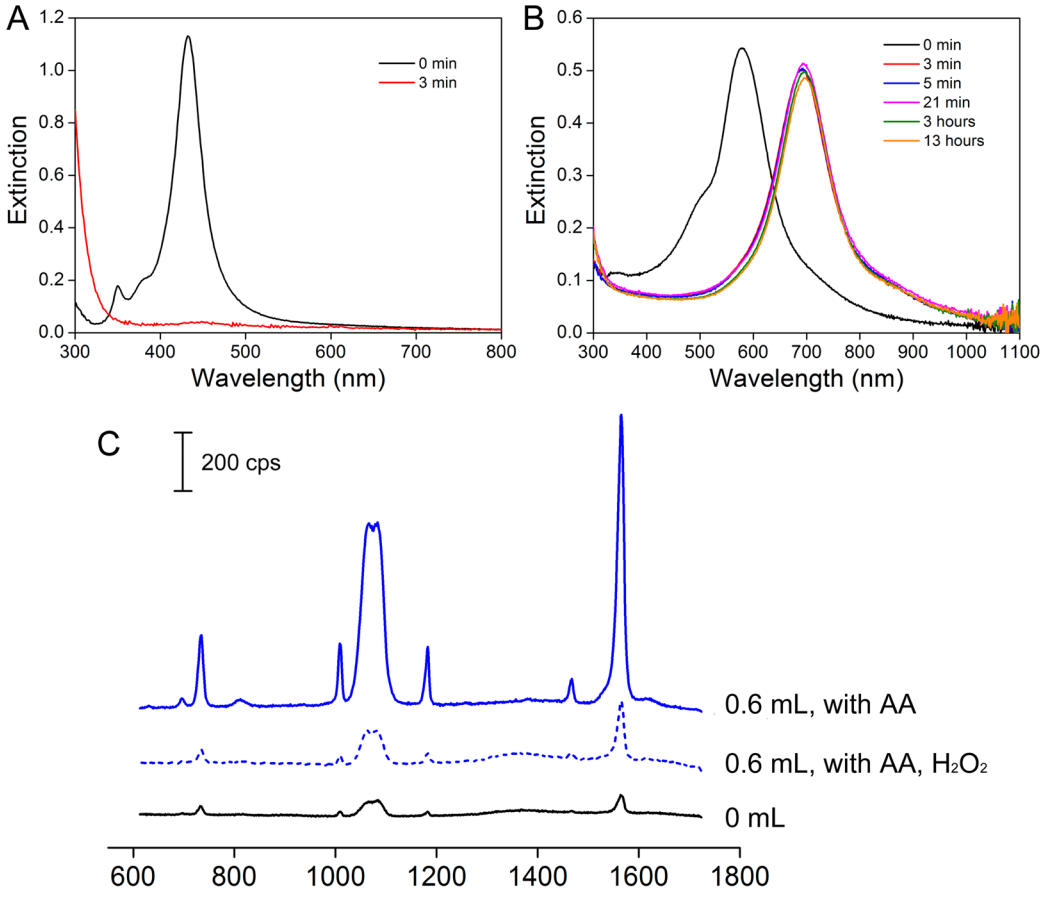

Figure 6. UV−vis spectra of (A) Ag nanocubes and (B) Ag−Au hollow nanostructures prepared by a reaction between Ag nanocubes and 0.6 mL of $HAuCl_4$ in the presence of AA before and after H_2O_2 etching. (C) Comparison of SERS activities for the Ag nanocubes, Ag−Au hollow nanostructures, and Ag−Au hollow nanostructures after H_2O_2 etching. The spectra were recorded with an excitation wavelength of 785 nm.

activity 33-fold stronger than the Ag−Au nanocages prepared by galvanic replacement without co-reduction. Our ICP-MS analysis indicates that the mole fractions of Ag were 76 and 65% for the Ag−Au hollow nanostructures and nanocages, respectively. Hence, the enrichment of Ag contributed to the enhancement in SERS.

It is worth noting that the SERS activity of the Ag−Au hollow nanostructures has a weak correlation with the LSPR peak position. As shown in Figure 4A, the LSPR peak was shifted from 436 to 596 nm during the transformation of Ag nanocubes into Ag−Au hollow nanostructures in the presence of AA. With excitation at 532 nm, the SERS intensity was attenuated because of plasmon damping, although there was a good overlap in terms of wavelength for the excitation source and LSPR peak position. In contrast, with excitation at 785 nm, away from the LSPR peak, the SERS activity of the Ag−Au hollow nanostructures was greatly enhanced. To evaluate the effect of LSPR peak position on the SERS activity further, we performed a direct comparison of Ag nanocubes with the Ag−Au hollow nanostructures and Ag−Au nanocages prepared from a reaction of Ag nanocubes with 0.6 mL of $HAuCl_4$ in the presence and absence of AA. Their corresponding LSPR peaks were located at 436 (nanocubes), 573 (nanoboxes), and 770 nm (nanocages), respectively. The nanocages showed the weakest SERS peak, although their LSPR peak overlapped the most with the 785 nm excitation. The weak correlation between SERS and LSPR peak position may reflect a change in the scattering to absorption cross sections as the composition and morphology were changed. Hence, we conclude that the composition, shape, and morphology of the Ag−Au hollow nanostructures play more significant roles in enhancing SERS with potential applications for noninvasive molecular detection and biomedical imaging in the near-infrared region.[40−43]

2.5. Chemical Stability of the Ag-Enriched Hollow Nanostructures. To evaluate the chemical stability of the Ag−Au hollow nanostructures, we performed a set of experiments by benchmarking against Ag nanocubes. Specifically, we reacted the Ag nanocubes with 0.6 mL of $HAuCl_4$ in the presence of AA, dispersed the samples in a 2.3% H_2O_2 solution for different periods of time up to 13 h, and recorded the UV−vis−NIR spectra as a function of time to monitor any possible changes in nanostructures. The original Ag nanocubes showed poor chemical stability in H_2O_2 with a complete drop in intensity for the LSPR peak at 436 nm within 3 min (Figure 6A). In contrast, upon mixing with H_2O_2, the LSPR peak of the Ag−Au hollow nanostructures was red-shifted from 573 to 693 nm within 3 min, and then the peak intensity remained unchanged for the next 13 h (Figure 6B). This result suggests that, upon removal of the pure Ag remaining in the interiors, the resultant Ag−Au hollow nanostructures embrace excellent chemical stability. More interestingly, the Ag−Au hollow nanostructures after H_2O_2 etching still showed a SERS activity 3-fold stronger than that of the Ag nanocubes (Figure 6C). It is reasonable that the loss of pure Ag from the interiors of Ag−Au hollow nanostructures because of H_2O_2 etching could result in some reduction of the SERS activity. This problem can be potentially

dx.doi.org/10.1021/am500506j | ACS Appl. Mater. Interfaces 2014, 6, 3750−3757

solved by optimizing the elemental composition of the Ag−Au walls to prevent the pure Ag from dissolution by H_2O_2.

3. CONCLUSIONS

We have demonstrated the transformation of Ag nanocubes into Ag−Au hollow nanostructures with enrichment in Ag content to improve their SERS activity. Specifically, we complemented the galvanic replacement reaction between Ag nanocubes and $HAuCl_4$ with a reducing agent to generate Au and Ag atoms through co-reduction. At the early stage, with the addition of a small amount of $AuCl_4^-$, we observed preferential deposition of the metal atoms at the corners and edges of Ag nanocubes without generating pits or pinholes on the side faces. As the amount of $AuCl_4^-$ increased, Ag atoms were constantly released as Ag^+ ions from the interiors of nanocubes because of a galvanic replacement reaction. The Ag^+ ions were immediately reduced back to Ag atoms together with the reduction of remaining $AuCl_4^-$ in the reaction solution. The newly formed Ag and Au atoms were co-deposited onto the Ag nanocubes, resulting in the formation of Ag−Au hollow nanostructures with >80% of the initial Ag being retained in the walls. We have evaluated the SERS properties of this novel class of Ag−Au hollow nanostructures. At 532 nm excitation, the SERS activity of the Ag−Au hollow nanostructures was weaker than that of the Ag nanocubes because of the plasmon dephasing associated with the interband transition of Au at 2.5 eV (~500 nm). In contrast, at 785 nm excitation to eliminate plasmon dephasing, we demonstrated the ability to enhance the SERS activity greatly by enriching the Ag content in the Ag−Au hollow nanostructures. Specifically, for the Ag−Au hollow nanostructures prepared with the addition of 0.6 mL of $AuCl_4^-$ and co-reduction, their SERS activity was 15- and 33-fold stronger than those of the Ag nanocubes and the Ag−Au nanocages prepared without co-reduction, respectively. Together with a considerably improved stability in an oxidizing environment, the Ag−Au hollow nanostructures embrace great potential for applications in SERS detection and imaging.

4. EXPERIMENTAL SECTION

Preparation of Ag Nanocubes. The Ag nanocubes were prepared using ethylene glycol (EG, J. T. Baker, lot no. G32B27) and silver trifluoroacetate (CF_3COOAg, Aldrich) as a solvent and a precursor to silver, respectively. In a typical synthesis, 5 mL of EG was introduced into a 100 mL round-bottomed flask (ACE Glass) and heated under magnetic stirring in an oil bath preset to 150 °C followed by quick injection of NaHS (0.06 mL, 3 mM in E G, Aldrich, 02326AH). After 2 min, HCl (0.5 mL, 3 mM in EG, Aldrich) was injected into the heated solution followed by the addition of poly(vinyl pyrrolidone) (PVP-55, MW ≈ 55 000, 1.25 mL, 20 mg/mL in EG, Aldrich). After another 2 min, CF_3COOAg (0.4 mL, 282 mM in EG) was added into the mixture. During the entire process, the flask was capped with a glass stopper except when adding reagents. The Ag nanocubes were obtained by quenching the reaction with an ice-water bath when the major LSPR peak of the Ag nanocubes was tuned to 436 nm. After centrifugation and washing with acetone and deionized (DI) water three times, the nanocubes were re-dispersed and stored in water.

Synthesis of Au−Ag Nanostructures in the Presence of AA. In a standard synthesis, 2 mL of 1 mM PVP-29 (MW ≈ 29 000) solution was injected into a 23 mL glass vial followed by an addition of 0.5 mL of 100 mM ascorbic acid and 10 μL of Ag nanocubes under magnetic stirring. Next, an $HAuCl_4$ aqueous solution (0.2 mM) was titrated at a rate of 0.02 mL/min by using a syringe pump. After reacting for 10 min, the product was collected by centrifugation at 15 000 rpm and washed with DI water four times for TEM characterization.

Synthesis of Au−Ag Nanostructures in the Absence of AA. In a typical synthesis, 2 mL of 1 mM PVP-29 (MW ≈ 29 000) solution was injected into a 23 mL glass vial followed by the addition of 0.5 mL of DI water and 10 μL of the Ag nanocubes under magnetic stirring. Next, an $HAuCl_4$ aqueous solution (0.2 mM) was titrated at a rate of 0.02 mL/min using a syringe pump at room temperature. After the completion of $HAuCl_4$ injection, the reaction was continued for 10 min. The product was collected by centrifugation at 15 000 rpm and washed with DI water four times prior to TEM characterization.

Instrumentation and Characterization. The UV−vis−NIR spectra were recorded using a Cary 50 spectrometer (Agilent Technologies, Santa Clara, CA). The measurements of Au and Ag content were conducted using an inductively coupled plasma mass spectrometer (ICP-MS, NexION 300Q, PerkinElmer, Waltham, MA). A routine centrifuge (Eppendorf 5430) and a high-speed centrifuge (Beckman Coulter Optima, Max-XP Ultracentrifuge) were used for the collection and washing of samples and the preparation of ICP-MS samples, respectively. Transmission electron microscopy (TEM) images were taken using a Hitachi HT-7700 microscope (Hitachi, Tokyo, Japan) operated at 120 kV. EDX analysis was performed using an FEI Tecnai G2 F20 S-Twin TEM equipped with an Oxford Inca x-sight spectrometer with a 1 mm^2 Si (Li) detector. EDX spectra were obtained under STEM mode using an accelerating voltage of 200 kV and a probe size of 1 nm. EDX mapping was conducted with 25 × 25 or 50 × 50 point scans at a 1500 ms dwell time.

Surface-Enhanced Raman Scattering Measurements. The Ag nanocubes and Au−Ag nanostructures were functionalized with a 0.6 mM ethanol solution of 1,4-BDT for 1 h. Next, the 1,4-BDT-functionalized nanostructures were washed with DI water twice before resuspension in water to achieve a concentration of approximately 2.6 × 10^{10} particles mL^{-1}. The Raman spectra were recorded from the solution phase using a Renishaw inVia Raman spectrometer coupled with a Leica microscope with a 100× objective lens. The excitation wavelength used was 785 nm equipped with a holographic notch filter with a grating of 2400 lines/mm or 532 nm equipped with a holographic notch filter with a grating of 1200 lines/mm. Data was collected from the solution phase with a collection time of 30 s for all samples and laser power at 50 (for 532 nm excitation) and 100 mW (for 785 nm excitation). A sample cell was constructed by attaching a polydimethylsiloxane (PDMS) block with a small hole, which can hold 20 μL of liquid sample, to a glass slide. A glass coverslip with a thickness of 170 μm was carefully placed on top to prevent the solvent from evaporating and to serve as a reference point, from which the focal plane was lowered 200 μm into the sample.

■ ASSOCIATED CONTENT

Ⓢ Supporting Information

TEM image of the Ag nanocubes used for all of the reactions described in this work; TEM images and illustrations (insets) of Ag nanocubes after reaction with different volumes of 0.2 mM $HAuCl_4$ aqueous solution in the absence of AA; and SERS spectra taken from 1,4-BDT adsorbed on Ag nanocubes before and after reacting with different volumes of 0.2 mM aqueous $HAuCl_4$ solution in the absence of AA. This material is available free of charge via the Internet at http://pubs.acs.org.

■ AUTHOR INFORMATION

Corresponding Author

*E-mail: dong.qin@mse.gatech.edu.

Notes

The authors declare no competing financial interest.

■ ACKNOWLEDGMENTS

This work was supported by start-up funds from the Georgia Institute of Technology. Part of the work was performed at the

Institute of Electronics and Nanotechnology (IEN) at the Georgia Institute of Technology, a member of the National Nanotechnology Infrastructure Network, which was partially supported by NSF (award no. ECS-0335765). Y.Y. was also partially supported by the China Scholarship Council. We thank Xin Zhao at the Georgia Institute of Technology for collecting ICP-MS data and Dr. Erwin M. Sabio at the University of Wyoming for collecting STEM and EDX mapping images.

REFERENCES

(1) Willets, K. A.; Van Duyne, R. P. Localized Surface Plasmon Resonance Spectroscopy and Sensing. *Annu. Rev. Phys. Chem.* **2007**, *58*, 267−297.
(2) Le Ru, E. C.; Etchegoin, P. G. Single-Molecule Surface-Enhanced Raman Spectroscopy. *Annu. Rev. Phys. Chem.* **2012**, *63*, 65−87.
(3) Le Ru, E. C.; Etchegoin, P. G. *Principles of Surface Enhanced Raman Spectroscopy: and Related Plasmonic Effects*; Elsevier: Boston, MA, 2009; Chapter 1, pp 1−27.
(4) Kneipp, K.; Wang, Y.; Kneipp, H.; Perelman, L. T.; Itzkan, I.; Dasari, R. R.; Feld, M. Single Molecule Detection Using Surface-Enhanced Raman Scattering (SERS). *Phys. Rev. Lett.* **1997**, *78*, 1667−1670.
(5) Qian, X.-M.; Nie, S. M. Single-Molecule and Single-Nanoparticle SERS: From Fundamental Mechanisms to Biomedical Applications. *Chem. Soc. Rev.* **2008**, *37*, 912−920.
(6) Mokosits, M. Surface-Enhanced Raman Spectroscopy: A Brief Retrospective. *J. Raman Spectrosc.* **2005**, *36*, 485−496.
(7) Kneipp, K.; Kneipp, H.; Itzkan, I.; Dasari, R. R.; Feld, M. S. Ultrasensitive Chemical Analysis by Raman Spectroscopy. *Chem. Rev.* **1999**, *99*, 2957−2975.
(8) Rycenga, M.; Cobley, C. M.; Zeng, J.; Li, W.; Moran, C. H.; Zhang, Q.; Qin, D.; Xia, Y. Controlling the Synthesis and Assembly of Silver Nanostructures for Plasmonic Applications. *Chem. Rev.* **2011**, *111*, 3669−3712.
(9) Xia, Y.; Halas, N. Shape-Controlled Synthesis and Surface Plasmonic Properties of Metallic Nanostructures. *MRS Bull.* **2005**, *30*, 338−348.
(10) Sherry, L. J.; Chang, S. H.; Schatz, G. C.; Van Duyne, R. P. Localized Surface Plasmon Resonance Spectroscopy of Single Silver Nanocubes. *Nano Lett.* **2005**, *5*, 2034−2038.
(11) McLellan, J. M.; Li, Z.-Y.; Siekkinen, A. R.; Xia, Y. The SERS Activity of a Supported Ag Nanocube Strongly Depends on Its Orientation Relative to Laser Polarization. *Nano Lett.* **2007**, *7*, 1013−1017.
(12) Rycenga, M.; Xia, X.; Moran, C.; Zhou, F.; Qin, D.; Li, Z.-Y.; Xia, Y. Generation of Hot Spots with Silver Nanocubes for Single-Molecule Detection by Surface-Enhanced Raman Scattering. *Angew. Chem., Int. Ed.* **2011**, *50*, 5473−5477.
(13) Jiang, X.; Zeng, Q.; Yu, A. Thiol-Frozen Shape Evolution of Triangular Silver Nanoplates. *Langmuir* **2007**, *23*, 2218−2223.
(14) Chen, Y.; Wang, C.; Ma, Z.; Su, Z. Controllable Colors and Shapes of Silver Nanostructures Based on pH: Application to Surface-Enhanced Raman Scattering. *Nanotechnology* **2007**, *18*, 325602.
(15) An, J.; Tang, B.; Zheng, X.; Zhou, J.; Dong, F.; Xu, S.; Wang, Y.; Zhao, B.; Xu, W. Sculpturing Effect of Chloride Ions in Shape Transformation from Triangular to Discal Silver Nanoplates. *J. Phys. Chem. C* **2008**, *112*, 15176−15182.
(16) Zhang, Q.; Ge, J.; Pham, T.; Goebl, J.; Hu, Y.; Lu, Z.; Yin, Y. Reconstruction of Silver Nanoplates by UV Irradiation: Tailored Optical Properties and Enhanced Stability. *Angew. Chem., Int. Ed.* **2009**, *121*, 3568−3571.
(17) Tang, B.; An, J.; Zheng, X.; Xu, S.; Li, D.; Zhou, J.; Zhao, B.; Xu, W. Silver Nanodisks with Tunable Size by Heat Aging. *J. Phys. Chem. C* **2008**, *112*, 18361−18367.
(18) McLellan, J. M.; Siekkinen, A. R.; Chen, J.; Xia, Y. Comparison of the Surface-Enhanced Raman Scattering on Sharp and Truncated Silver Nanocubes. *Chem. Phys. Lett.* **2006**, *427*, 122−126.
(19) Gutes, A.; Maboudian, R.; Carraro, C. Gold-Coated Silver Dendrites as SERS Substrates with an Improved Lifetime. *Langmuir* **2012**, *28*, 17846−17850.
(20) Gao, C.; Lu, Z.; Liu, Y.; Zhang, Q.; Chi, M.; Cheng, Q.; Yin, Y. Highly Stable Silver Nanoplates for Surface Plasmon Resonance Biosensing. *Angew. Chem., Int. Ed.* **2012**, *51*, 5629−5633.
(21) Mallin, M. P.; Murphy, C. J. Solution-Phase Synthesis of Sub-10 nm Au-Ag Alloy Nanoparticles. *Nano Lett.* **2002**, *2*, 1235−1237.
(22) Link, S.; Wang, Z. L.; El-Sayed, M. A. Alloy Formation of Gold-Silver Nanoparticles and the Dependence of the Plasmon Absorption on Their Composition. *J. Phys. Chem. B* **1995**, 3529−3533.
(23) Sun, Y.; Xia, Y. Mechanistic Study on the Replacement Reaction between Silver Nanostructures and Chloroauric Acid in Aqueous Medium. *J. Am. Chem. Soc.* **2004**, *126*, 3892−3901.
(24) Métraux, G. S.; Cao, Y. C.; Jin, R.; Mirkin, C. A. Triangular Nanoframes Made of Gold and Silver. *Nano Lett.* **2003**, *3*, 519−522.
(25) Olson, T. Y.; Schwartzberg, A. M.; Orme, C. A.; Talley, C. E.; O'Connell, B.; Zhang, J. Z. Hollow Gold−Silver Double-Shell Nanospheres: Structure, Optical Absorption, and Surface-Enhanced Raman Scattering. *J. Phys. Chem. C* **2008**, *112*, 6319−6329.
(26) Mahmoud, M. A.; El-Sayed, M. A. Metallic Double Shell Hollow Nanocages: The Challenges of Their Synthetic Techniques. *Langmuir* **2012**, *28*, 4051−4059.
(27) Hao, E.; Li, S.; Bailey, R. C.; Zou, S.; Schatz, G. C.; Hupp, J. T. Optical Properties of Metal Nanoshells. *J. Phys. Chem. B* **2004**, *108*, 1224−1229.
(28) Rycenga, M.; Hou, K. K.; Cobley, C. M.; Schwartz, A. G.; Camargo, P. H. C.; Xia, Y. Probing the Surface-Enhanced Raman Scattering Properties of Au−Ag Nanocages at Two Different Excitation Wavelengths. *Phys. Chem. Chem. Phys.* **2009**, *11*, 5903−5908.
(29) Jana, N.; Gearheart, L.; Murphy, C. J. Wet Chemical Synthesis of Silver Nanorods and Nanowires of Controllable Aspect Ratio. *Chem. Commun.* **2001**, *7*, 617−618.
(30) Rodríguez-González, B.; Burrows, A.; Watanabe, M.; Kiely, C. J.; Liz-Marzán, L. M. Multishell Bimetallic AuAg Nanoparticles: Synthesis, Structure and Optical Properties. *J. Mater. Chem.* **2005**, *15*, 1755−1759.
(31) Aherne, D.; Gara, M.; Kelly, J. M.; Gun'ko, Y. K. From Ag Nanoprisms to Triangular AuAg Nanoboxes. *Adv. Funct. Mater.* **2010**, *20*, 1329−1338.
(32) Mohammad, M. S.; Bosman, M.; Cao, S.; Huang, X.; Saadat, S.; Matinsson, E.; Aili, D.; Tay, Y. Y.; Liedberg, B.; Loo, S. C. J.; Zhang, H.; Boey, F.; Xue, C. Gold Coating of Silver Nanoprisms. *Adv. Funct. Mater.* **2012**, *22*, 849−854.
(33) McEachran, M.; Keogh, D.; Pietrobon, B.; Cathcart, N.; Gourevich, I.; Coombs, N.; Kitaev, V. Ultrathin Gold Nanoframes through Surfactant-Free Templating of Faceted Pentagonal Silver Nanoparticles. *J. Am. Chem. Soc.* **2011**, *133*, 8066−8069.
(34) Hong, X.; Wang, D.; Cai, S.; Rong, H.; Li, Y. Single-Crystalline Octahedral Au−Ag Nanoframes. *J. Am. Chem. Soc.* **2012**, *134*, 18165−18168.
(35) DeSantis, C. J.; Bower, M. M.; Skrabalak, S. E. Seed-Mediated Co-reduction: A Versatile Route to Architecturally Controlled Bimetallic Nanostructures. *ACS Nano* **2012**, *6*, 2617−2628.
(36) Chen, S.; Jenkins, S. V.; Tao, J.; Zhu, Y. M.; Chen, J. Anisotropic Seeded Growth of Cu−M (M = Au, Pt, or Pd) Bimetallic Nanorods with Tunable Optical and Catalytic Properties. *J. Phys. Chem. C* **2013**, *117*, 8924−8932.
(37) Johnson, P.; Christy, R. Optical Constants of the Noble Metals. *Phys. Rev. B: Solid State* **1972**, *6*, 4370−4379.
(38) Xia, X.; Jie, Z.; Oetjen, L. K.; Li, Q.; Xia, Y. Quantitative Analysis of the Role Played by Poly(vinyl pyrrolidone) in Seed-Mediated Growth of Ag Nanocrystals. *J. Am. Chem. Soc.* **2012**, *134*, 1793−1801.
(39) Xie, S.; Lu, N.; Xie, Z.; Wang, J.; Kim, M. J.; Xia, Y. Synthesis of Pd-Rh Core−Frame Concave Nanocubes and Their Conversion to Rh Cubic Nanoframes by Selective Etching of the Pd Cores. *Angew. Chem., Int. Ed.* **2012**, *51*, 10266−10270.

(40) Keren, S.; Zavaleta, C.; Cheng, Z.; Zerda, A.; Gheysens, O.; Gambhir, S. S. Noninvasive Molecular Imaging of Small Living Subjects Using Raman Spectroscopy. *Proc. Natl. Acad. Sci. U.S.A.* **2008**, *105*, 5844−5849.
(41) Alvarez-Puebla, R. A.; Liz-Marzan, L. M. SERS-Based Diagnosis and Biodetection. *Small* **2010**, *6*, 604−610.
(42) Koo, H.; Huh, M. S.; Ryu, J. H.; Lee, D.; Sun, I.; Choi, K.; Kim, K.; Kwon, I. C. Nanoprobes for Biomedical Imaging in Living Systems. *Nano Today* **2011**, *6*, 204−220.
(43) Schlucker, S. SERS Microscopy: Nanoparticle Probes and Biomedical Applications. *ChemPhysChem* **2009**, *10*, 1344−1354.